CAD OF STACKED PATCH ANTENNAS THROUGH MULTIPURPOSE ADMITTANCE MATRICES FROM FEM AND NEURAL NETWORKS

Juan Córcoles, Miguel A. González, and Juan Zapata
Departamento de Electromagnetismo y Teoría de Circuitos,
Universidad Politécnica de Madrid, Ciudad Universitaria s/n, 28040
Madrid, Spain; Corresponding author: corcoles@etc.upm.es

ABSTRACT: *In this work, a novel computer-aided design methodology for probe-fed, cavity-backed, stacked microstrip patch antennas is proposed. The methodology incorporates the rigor of a numerical technique, such as finite element methods, which, in turn, makes use of a newly developed procedure (multipurpose admittance matrices) to carry out a full-wave analysis in a given structure in spite of certain physical shapes and dimensions not yet being established. With the aid of this technique, we form a training set for a neural network, whose output is the desired response of the antenna according to the value of design parameters. Last, taking advantage of this neural network, we perform a global optimization through a genetic algorithm or simulated annealing to obtain a final design. The proposed methodology is validated through*

Key words: *computer-aided design; finite element methods; neural networks; optimization algorithms; stacked microstrip antennas*

1. INTRODUCTION

Microstrip patch antennas have been focusing the attention of researchers for a long time, because they are easy to use in different configurations and their versatility in achieving a wide variety of responses One of the most usual configurations of microstrip antennas can be found and this is the one where two or more patches are stacked within several dielectric layers. These patches are intended to introduce resonances, thus being able to increase bandwidth and have a broadband/multiband antenna Circuit models are not accurate enough to carry out a rigorous analysis of these structures, and the use of a full-wave numerical technique then being required, such as finite-element methods (FEM), finite-difference methods, method of moments, or hybrid methods. However, until not so long ago, the time consumed by these techniques made them prohibitive when addressing a new design, pushing them into the background, and recovering them only for validation purposes. On the other hand, not only there have been astounding advances in the field of computation, but there have also been promising achievements toward full-wave optimization, in the sense of newly developed clever procedures, working as novel standalone methods or applied to the aforementioned classic numerical techniques.

In this work, we propose a novel computer-aided design (CAD) methodology for the design of probe-fed stacked microstrip patch antennas, which incorporates the rigor of a contrasted numerical technique, such as FEM, and, in turn, makes use of the powerful feature of the so-called domain decomposition method, implemented in two different ways (namely modal and artificial ports), to render the computer simulation highly efficient through the calculation of multipurpose admittance matrices (MAM) To be able to perform an optimization in our design process, two well-known advanced mathematical techniques have been used: neural networks (NN) and global optimization algorithms. To validate the methodology, we present a real design, a broadband microstrip antenna consisting of cavity-backed stacked patches, whose numerical predictions are compared to measurements.

2. THEORY

A canonical representation of the antenna being designed is shown in Figure 1. It basically consists of T-stacked patches within L-dielectric layers, all of which are enclosed in a cavity. The lower patch is fed via a probe. The shape and location of the patches, placed parallel to the x–y plane as shown in Figure 1, can be arbitrary. In the same way, the profile of the cavity along the z direction, as well as its cross-sectional shape (in planes perpendicular to that direction), can also be piecewise arbitrary as shown in the figure. To make our design, we must first decide on some geometrical constraints and, according to them, the parameters and their associated ranges of values involved in the design $x_1, x_2, \ldots, x_I$ must be selected. This choice is critical, because it requires the necessary knowledge of which ones really do affect the desired output of the antenna. This output, which we will refer to as y, should be directly related to any physical response of the antenna (directive gain, matching, input-match bandwidth, ...) or a combination of them. We have divided the CAD methodology into

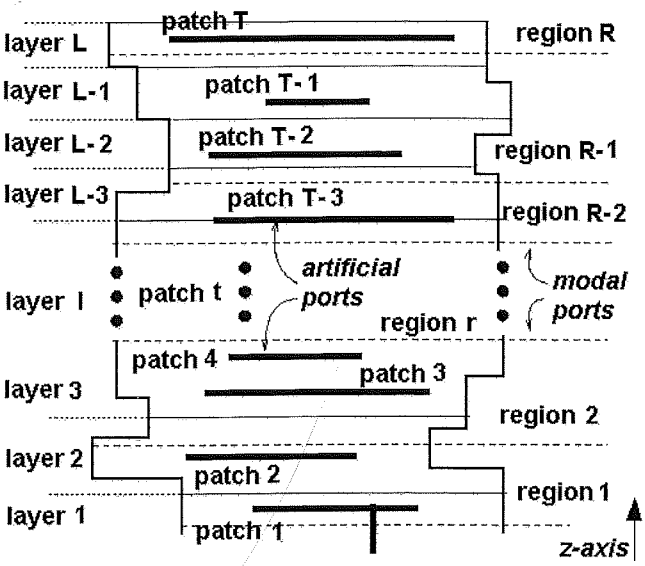

Figure 1 Canonical geometry of the antenna to be designed

three steps, which will be described throughout the following subsections.

2.1. *Multipurpose Admittance Matrices from FEM*

Segmentation Finite Element via Lanczos-Padé (SFELP) is a methodology to analyze microwave passive devices It is based on the domain decomposition technique, the FEM, and the generalized scattering matrix (GAM). The procedure has been extended to the analysis of radiating structures [8, 9] through the inclusion of a spherical computation domain where a spherical modal expansion (on what is called a spherical port) is performed to characterize the radiating region. The FEM simulation is synergized by considering modal field expansion and consequently a GAM results, that is, a matrix-valued transfer function. This simulation can be carried out on a frequency-by-frequency basis or, on the other hand, make use of a reduced-order model, namely a Padé approximation scheme via the Lanczos process.

One of the most powerful features of SFELP is its capability to segment a given structure in different regions delimited by modal ports where modal expansions of the electromagnetic fields are used. The application of the hybrid 3D-FEM to each region provides the GAM that describes it, which relates complex modal coefficients on the considered ports in that region. The partial GAMs can be assembled analytically, with no additional numerical effort, by connecting the desired ports through a section with an arbitrary length of a canonical transmission line (such as a rectangular or circular waveguide or a coaxial line) or a transmission line, which has been numerically characterized by a 2D-FEM. This feature allows the design methodology to modify any distance along the z-axis in Figure 1 easily by dividing the whole structure into R regions, allowing the variation of parameters such as dielectric thicknesses or separation between patches.

In the MAM approach , a further exploitation of the matrix-valued transfer function describing electromagnetic behavior is considered. In addition to the inclusion of modal ports in the analysis domain, new computational domain ports (artificial ports) are taken into account. The aim of this new port definition is to obtain the aforementioned matrix-valued transfer function even though some boundary field distributions are not yet set. In other words, it is able to carry out a full-wave analysis in a given structure in spite of certain physical shapes and dimensions not yet

being established and, afterward, to make it possible to consider conducting strips/slots in the computational domain with ease by causing field discontinuities/continuities by means of simple manipulations of the matrix-valued transfer function.

we can define both the tangential electric and magnetic vector field on an artificial port by taking advantage of the FEM context as an expansion of piecewise (PCW) basis functions and their associated complex coefficients.

This way, following a similar scheme we can arrive at a matrix-valued transfer function, which stands for the relationship between the modal fields in the M modal ports and the PCW functions in the A artificial ports lying on the boundary of our domain:

$$(\mathbf{i} \quad \mathbf{I}) = \frac{-jk}{\eta_0}\mathbf{d}^{-1}\mathbf{B}^{\mathrm{T}}(\mathbf{K} - k^2\mathbf{M})\mathbf{B}\begin{pmatrix}\mathbf{v}\\ \mathbf{V}\end{pmatrix} \tag{1}$$

$$\mathbf{i} = (\mathbf{i}_1^{\mathrm{T}} \ldots \mathbf{i}_m^{\mathrm{T}} \ldots \mathbf{i}_M^{\mathrm{T}}) \tag{2}$$

$$\mathbf{I} = (\mathbf{I}_1^{\mathrm{T}} \ldots \mathbf{I}_a^{\mathrm{T}} \ldots \mathbf{I}_A^{\mathrm{T}}) \tag{3}$$

$$\mathbf{v} = (\mathbf{v}_1^{\mathrm{T}} \ldots \mathbf{v}_m^{\mathrm{T}} \ldots \mathbf{v}_M^{\mathrm{T}}) \tag{4}$$

$$\mathbf{V} = (\mathbf{V}_1^{\mathrm{T}} \ldots \mathbf{V}_a^{\mathrm{T}} \ldots \mathbf{V}_A^{\mathrm{T}}) \tag{5}$$

where $\mathbf{v}_m$,$\mathbf{i}_m$,$\mathbf{V}_a$, and $\mathbf{I}_a$ are coefficient vectors of the tangential electric and magnetic field on the modal port m and the tangential electric and magnetic field on the artificial port a, , respectively; $\mathbf{K}$, and $\mathbf{M}$ are sparse symmetric matrices, $\mathbf{B}$ is a sparse matrix, and $\mathbf{d}$ is a block diagonal matrix. Hence, a full-wave admittance-type matrix, namely a multipurpose admittance matrix arises, and, as a result, we are able to deal with a multiport network, where the electromagnetic complexity in the analysis domain has been removed. This way, multiple different physical shape and dimension analysis can be obtained straightforwardly from the same MAM without the need to carry out any other FEM simulation every time a parameter is varied. So far, the full-wave transfer function of a variety of specific device realizations requiring only one large sparse FEM stiffness matrix inversion-like computation is obtained. In this full-wave network, straightforward elementary circuit manipulation can be carried out in the artificial ports, all with a direct electromagnetic counterpart in the actual structure in the form of a GAM, removing all physical uncertainties. For example, we can nullify the tangential electric field, thus rendering an artificial port short circuit, by simply imposing $\mathbf{V}_a = 0$ on the desired artificial port a in (1), which is equivalent to setting a metallic surface on such port. Analogously, we may impose $\mathbf{I}_a = 0$ to have an artificial port a open circuit, which is equivalent to setting a magnetic wall on the surface defined by such port (this possibility is not necessary in the proposed methodology). Finally, we can impose the field continuity across two artificial ports a and b defined on the two sides of the same portion of a surface, both sharing the same mesh, by setting $\mathbf{V}_a = \mathbf{V}_b, \mathbf{I}_a = -\mathbf{I}_b$ in (1). In this way, we can insert and remove flexibly metallic surfaces in the domain of analysis through simple matrix manipulations. This feature allows the design methodology to vary easily parameters directly related to the shape and location in the x–y plane of a patch where pairs of artificial ports have been defined on each side of the patch surface. For example, Figure 2 shows the different cases for two typical geometries, a circular patch made up of two circular ports, A and B, and two ring artificial ports, F and G; and a rectangular patch made up of two triangular artificial ports, A and B, and two irregular quadrilateral artificial ports, F and G. As

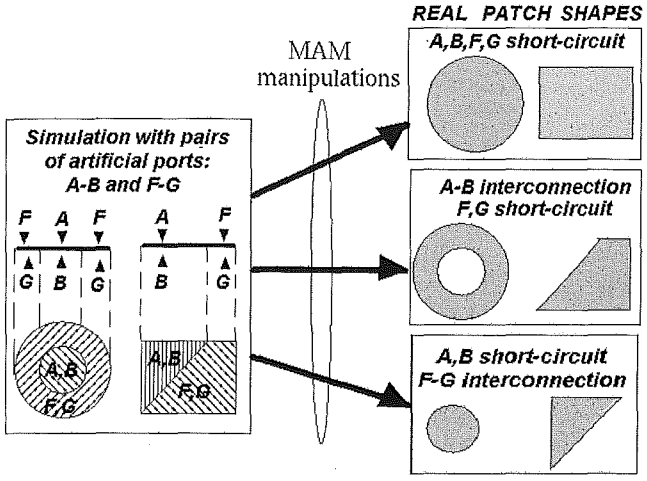

Figure 2 Example of the possibilities given by the artificial ports for two typical patch geometries

previously stated, these two pairs of artificial ports (A and B, and F and G) are defined on the same portion of the surface but on different sides. By connecting each pair of artificial ports or letting them short circuit (through the appropriate MAM manipulations), we can easily vary the shape and dimensions of these patch geometries, having the possibilities shown in Figure 2.

In this way, the first step of the CAD methodology, which is intended to bear the majority of the computational burden, can be summarized in Figure 3. As can be seen, we first calculate the MAM corresponding to the R regions we have divided our whole structure delimited by the modal ports in Figure 1, which exactly require only R FEM simulations. To model the shape of the patches and their location in the x–y plane flexibly, we use several pairs of artificial ports inside each region as shown in Figure 1. By properly connecting these latter pairs of ports or letting them short circuit, we can produce S_r GAMs for region r, each one corresponding to a different shape and/or location of the aforementioned patches, thus being able to vary the parameters associated to these shapes and locations without the need of carrying out any more FEM simulations. We can then finally assemble all combinations of the GAMs belonging to all regions via the analytical connection of modal ports through sections of transmission lines, which correspond to a variation in substrate thicknesses. This way, several GAMs (which can easily be converted into GSMs if needed), which represent the results of carrying out a FEM simulation for each different combination of different values of design parameters $x_1, x_2, \ldots, x_I$ belonging to discrete sets of values $\mathbf{X}_i$, are easily obtained with an affordable computational effort.

2.2. Neural Network and Global Optimization

The purpose of the second step of the proposed CAD methodology (training a neural network) is to obtain a fast mathematical tool that provides a value z of the response immediately for an arbitrary value of the design parameters, which would be similar to the value y given by a full-wave simulation, but without the need to carry it out. This fact can be used to have a large search space (in theory, as large as desired) with enough points to find the global maximum/minimum through the application of a global optimization algorithm. Note that, without the inclusion of this second step, the search space of the global optimization algorithm would be constrained to the discrete sets of values $\mathbf{X}_i$ (P points) given directly by the first step, which would require an increase in the number of FEM simulations to have a large enough search space.

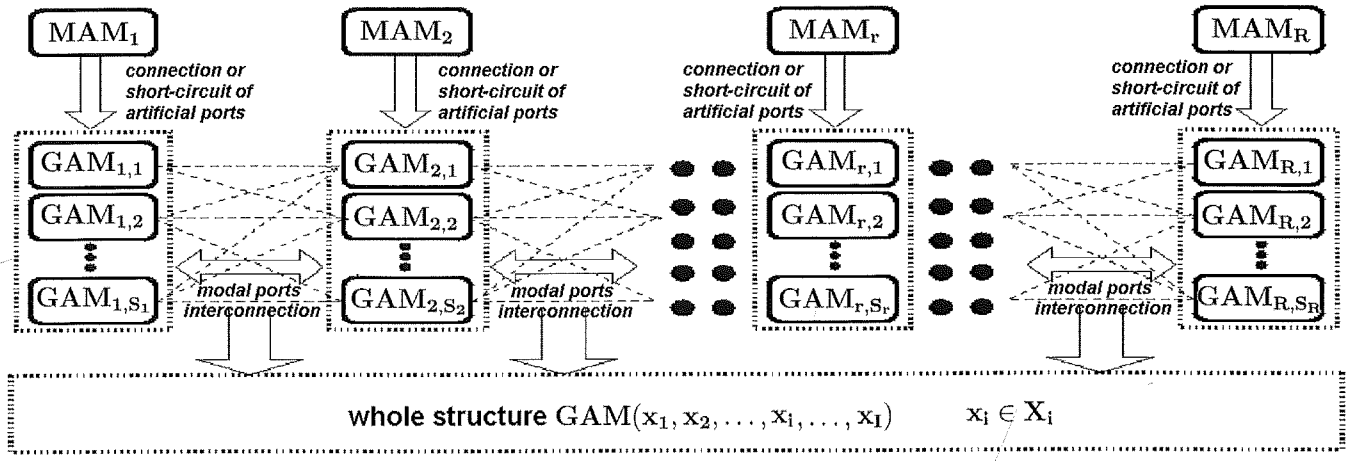

Figure 3 Graphical description of the first step of the CAD methodology: application of MAM

Once we have carried out the first step of our CAD methodology, we have a training set for the neural network consisting of P patterns, corresponding to the discrete sets of values $\mathbf{X}_i$ of the parameters (directly taken from the MAM simulation). Each pattern p has an input $x_1^p, \ldots, x_i^p, \ldots, x_I^p$ and an output y^p. For our CAD methodology, we have used a simple multilayer perceptron feedforward neural network [4], with an input layer (with normalized inputs), a hidden layer (with H hidden neurons), and an output layer with a linear neuron, which directly provides the output. Each neuron belonging to the hidden layer has been implemented as a perceptron with an activation function of tan h type. For the training, we carry out a random sequential learning based on the error backpropagation algorithm As for the learning rates, we have chosen a simple varying learning rate, which decays with the number of epochs [4].

To carry out the third step of the methodology (global optimization), we use three different techniques: a classic genetic algorithm (GA), a micro-GA, and a simulated annealing scheme (SA). The micro-GA is a very small population GA. The GA and micro-GA implementation used in the proposed CAD methodology can be found An adaptive version of the SA algorithm to perform several circuit and antenna designs has also been used.

3. APPLICATION: BROADBAND STACKED CIRCULAR PATCHES FOR DCS AND UMTS BANDS

To validate our methodology, we have carried out the design of a broadband antenna covering both the DCS and UMTS bands from 1710 to 2170 MHz. The geometry of this antenna is shown in Figure 4 and consists of two stacked circular patches embedded in a circular cylindrical cavity. The lower patch lies on a substrate, and it is excited via the inner conductor of a coaxial connector situated at an offset from the centre. The upper patch is coupled through air, because it is printed at the bottom of a superstrate, which, in turn, lies on top of the cavity, whose profile has been lowered to that effect. This geometry was intentionally conceived to facilitate its physical implementation.

A good starting point for a similar design (with no superstrate) It is based on how each antenna parameter affects the impedance behavior, given by a loop on the Smith chart due to the presence of two resonances corresponding to the two stacked patches. Following these rules, we have chosen the parameters involved in the design to be the radii of the lower and upper patches, and the distance between both patches, because the combination of these three parameters is enough to have a wide range in controlling the input impedance in the desired band. In addition, the values for the substrate permittivity and thickness have been adjusted to the commercial ones closest to those given . Given the fact that these initial values do not account for the presence of a superstrate, used intentionally in our design for a matter of ease in the construction of the antenna as well as a possible cover, we have chosen the values of the permittivity and thickness of this superstrate to be as small as possible at the considered frequencies, taking into account the mechanical issues within the commercial range of values. The coaxial feed has been chosen to be a 50-Ω N-type connector. In this way, we have set the parameters of the antenna in Figure 4 to the ones shown in Table 1, where λ_0 is the free-space wavelength and $\lambda_g = \lambda_0/\sqrt{\varepsilon_{r1}}$.

3.1. MAM Simulations

The antenna is segmented into two regions, which are separated by a circular port, as shown in Figure 4, where a modal expansion with 75 modes has been used. One region contains the coaxial feeding, the substrate, the lower patch and part of the cavity, and the other one comprises the rest of the cavity, the upper patch, the superstrate, and a semispherical port to model the radiating characteristics, because the cavity is recessed in an infinite metallic plane. Thus, the distance between patches can be easily varied by the analytical procedure of connecting both regions through a circular waveguide of the desired length. When calculating the MAM of each region, we have used 10 pairs of concentric artificial ports in each patch surface, which means that 11 different values,

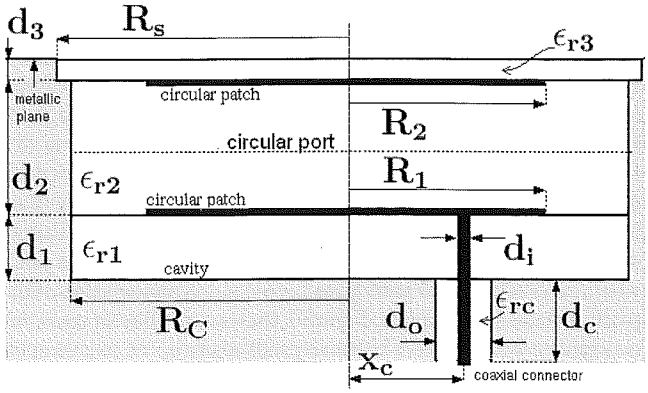

Figure 4 Geometry and parameters of the antenna to be designed

TABLE 1. Values of the Parameters of Antenna in Figure 4

Parameter	Value (cm)	Idea According to [2]
ϵ_{r1}	2.5	2.2
ϵ_{r2}	1	1.07
ϵ_{r3}	2.17	-
ϵ_{rc}	1.8998	-
R_1	To be designed	0.25 λ_g at central frequency = 2.61 cm
R_2	To be designed	0.25 λ_g at central frequency = 2.61 cm
R_C	4.5	-
R_s	4.7	-
d_1	0.635	0.04 λ_0 at central frequency = 0.619 cm
d_2	To be designed	0.06 λ_0 at central frequency = 0.928 cm
d_3	0.1524	-
d_c	0.3	-
d_i	0.31	-
d_o	0.98	-
x_c	1.9	To yield 250 Ω at resonance in the lower edge of the band w/o upper patch

ranging uniformly (in steps of 0.15 cm) from 2.5 cm to 4.0 cm, for each radius will be available according to different combinations of artificial port connections and short circuits. All dimensions and dielectric permittivities shown in Table 1 for Figure 4 are considered in the simulation. To complete the training set, we have chosen to vary the distance between patches in steps of 0.125 cm from 0.75 to 2.00 cm, which provides 11 different values. Note that our training set consists of 1331 patterns per frequency, which with a classic FEM approach would require such a number of full-wave simulations, thus resulting in a prohibitive time. In our case, only two FEM numerical simulations have been carried out (one per region), and the rest of the computational effort is reduced to 11 artificial port matrix manipulations per region and their corresponding modal interconnections.

3.2. *Neural Network Training*

The output of the neural network has been chosen to be the magnitude of the reflection coefficient $|S_{11}|$ directly. We have placed 45 hidden neurons in the network, and because, in this example, we have used a frequency-by-frequency scheme covering the desired band instead of making use of the reduced order model, the neural network has been trained for each point of frequency analyzed in the MAM simulation. An automatic stop criterion has been defined when the root mean square in $|S_{11}|$ changes in less than 0.01 for 500 consecutive epochs. Otherwise, the training continues until reaching a maximum of 10000 epochs. The neural network training takes an average number of 1900 epochs per point of frequency. In the computer used for this training (Pentium 2.8 GHz), this means less than 20 min for the whole band.

3.3. *Optimization Phase*

Once the neural network has been trained, we proceed to the optimization phase. In this case, we set the possibilities for each radius to 128 (from 2.49 cm to 3.76 cm in steps of 0.01 cm) and the variations for the distance between patches to 128 (from 0.75 cm to 2.02 cm in steps of 0.01 cm). This makes a search space of 2,097,152 possibilities. In the GA and micro-GA, the fitness function has been chosen as the maximum value of the reflection coefficient in the desired band, $\max_f|S_{11}(f)|$. Analogously, for the SA, the cost function has been set to $1 - \max_f|S_{11}(f)|$. For the classic and micro-GA, we have respectively chosen a population

TABLE 2. Results for the Different Optimization Algorithms

	SA	GA	Micro-GA
R_1 (cm)	2.88	2.88	2.88
R_2 (cm)	2.84	2.84	2.80
d_2 (cm)	1.49	1.47	1.48
$\max_f \|S_{11}(f)\|$	0.2964	0.3057	0.3086
Evaluations	13723	2550	1000

size of 50 and 5 individuals for a maximum number of generations of 51 and 200. The results for the design of the three global optimization algorithms are shown in Table 2. The similarity of the solutions reached by all of them can be seen, especially between the classic GA and SA. One has to take into account that SA has a sophisticated automatic stop criterion, which makes it to require many more evaluations of the cost function than the GA or micro-GA do, because they both stop simply when a maximum number of iterations is reached. In any case, because the evaluation of the cost function for any combination of the design parameters just requires their introduction in the neural network, whose output is instantaneously obtained, the time used in the optimization can be said to be ridiculous (just a few seconds in the case of SA, less than one second for the GAs).

3.4. *Final Design*

We have constructed the design given by the classic GA using a finite circular metallic plane with 36 cm of diameter. Figure 5 shows a photo of the antenna in which the superstrate has been removed from its original position to see the lower patch and the cavity. The upper patch is the one shown at the bottom of the figure. Figure 6 shows the measured VSWR of the antenna against the results given by the neural network, both being in agreement. As can be seen, a 26% relative bandwidth at VSWR = 2, covering the desired bands, has been achieved. The radiation patterns at different frequencies have also been computed from a full-wave simulation of the design, showing, as expected, a good uniformity throughout the desired frequency band.

4.5. *Other Designs*

As has been previously said, once the neural network is trained for this specified topology, the optimization phase is just a matter of

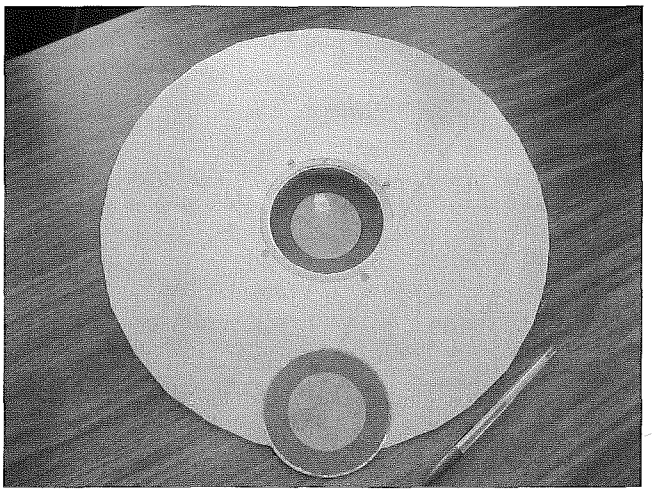

Figure 5 Photograph of the constructed and measured antenna. The superstrate has been removed and the upper patch is the one shown at the bottom

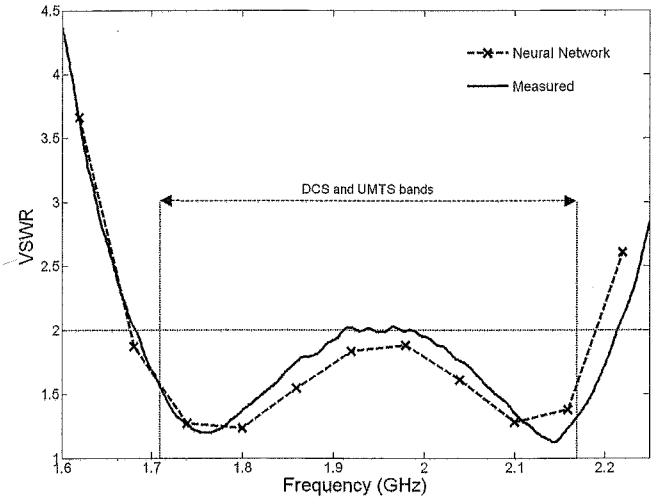

Figure 6 Measured and computed VSWR for the designed antenna showing a 26% relative bandwidth at VSWR = 2

one second for the classic GA. Thus, changing the fitness function so that it covers just the UMTS band, we have obtained another design for this band (1900–2170 MHz), whose design values are $R_1 = 2.74$ cm, $R_2 = 2.49$ cm, and $d_2 = 1.86$ cm. The return loss according to the neural network of this last design can be seen against the design covering both bands in Figure 7, which shows how a better matching can be achieved by reducing the band, moving from a design of ~26% of relative bandwidth at −10 dB to a one with ~13% of relative bandwidth at −20 dB.

4. CONCLUSIONS

A novel computer-aided design methodology for the design of probe fed, cavity backed, stacked microstrip patch antennas has been presented. It makes use of different advanced mathematical tools: a hybrid numerical–analytical method based on FEM to characterize the electromagnetic behavior inside any structure rigorously; a neural network to be able to reproduce the results such a method would yield with speed, ease, and reliability; and a global optimization algorithm to reach a solution to the design as close to the desired specifications as possible. Once we have trained the neural network to yield the desired response of a given topology, we can obtain a design by changing these specifications in the optimization phase, whose computational effort can be said to be negligible. To validate the methodology, a real design has been carried out showing good agreement between numerical results and measured values.

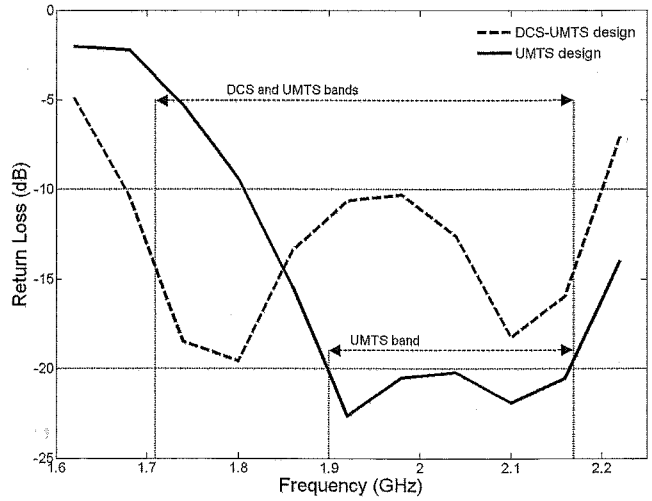

Figure 7 Return loss for the two different designs carried out with the methodology according to the topology of Figure 4

REFERENCES

R. Garg, P. Bhartia, I. Bahl, and A. Ittipiboon, Microstrip Antenna Design Handbook, Artech House, Norwood, MA, 2001.

R. B. Waterhouse, Design of probe-fed stacked patches, IEEE Trans Antennas Propag 47 (1999), 1780-1784.

V. de la Rubia and J. Zapata, MAM-A multi-purpose admittance matrix for antenna design via the finite element method, IEEE Trans Antennas Propag 55 (2007), 2276-2286.

S. Haykin, Neural networks: A comprehensive foundation, 2nd ed., Prentice Hall, Upper Saddle River, NJ, 1998.

D. E. Goldberg, Genetic Algorithms in Search, Optimization, and Machine Learning, Addison-Wesley, Reading, MA, 1989.

J. Rubio, J. Arroyo, and J. Zapata, Analysis of passive microwave circuits by using a hybrid 2-D and 3-D finite-element mode-matching method, IEEE Trans Microwave Theory Tech 47 (1999), 1746-1749.

J. Rubio, J. Arroyo, and J. Zapata, SFELP—An efficient methodology for microwave circuit analysis, IEEE Trans Microwave Theory Tech 49 (2001), 509-516.

J. Rubio, M. A. González, and J. Zapata, Analysis of cavity-backed microstrip antennas by a 3-D finite element/segmentation method and a matrix Lanczos-Padé algorithm (SFELP), IEEE Antennas Wireless Propag Lett 1 (2002), 193-195.

J. Rubio, M. A. González, and J. Zapata, Generalized-scattering-matrix analysis of a class of finite arrays of coupled antennas by using 3-D FEM and spherical mode expansion, IEEE Trans Antennas Propag 53 (2005), 1133-1144.

D. E. Rumelhart, G. E. Hinton, and R. J. Williams, Learning internal representations by error propagation, In: D. E. Rumelhart, J. L. McClelland, et al. (Eds.), Parallel distributed processing, Vol. 1: Foundations, MIT Press, Cambridge, 1987, pp. 318-362.

P. Brierley and B. Batty, Data mining with neural networks—An applied example in understanding electricity consumption patterns, In: M. Bramer (Ed.), Knowledge discovery and data mining, Institution of Electrical Engineers, Stevenage, UK, 1999, pp. 240-303.

P. Brierley, Neural network software, 2006 [Online]. Available at http://www.philbrierley.com/.

D. L. Carroll, Fortran genetic algorithm, 1999 [Online]. Available at http://cuaerospace.com/carroll/ga.html.

K. Krishnakumar, Micro-genetic algorithms for stationary and non-stationary function optimization, In: Proceedings of the SPIE (Intelligent Control and Adaptive Systems, Vol. 1196), Philadelphia, PA, Nov 7–8, 1990, pp. 289-296.

R. H. J. M. Otten and L. P. P. P. van Ginneken, The Annealing Algorithm, Deventer, The Netherlands, 1989.

J. Monge, J. M. Gil, and J. Zapata, Optimization of arbitrarily shaped H-plane passive microwave devices through finite elements and the annealing algorithm, Microwave Opt Technol Lett 46 (2005), 360-366.

J. Monge, J. M. Cid, J. M. Gil, and J. Zapata, Optimization of arbitrarily shaped dielectric axisymmetric horns through finite elements and the annealing algorithm, Microwave Opt Technol Lett 48 (2006), 1074-1079.

J. M. Gil, J. Monge, J. Rubio, and J. Zapata, A CAD-oriented method to analyze and design radiating structures based on bodies of revolution by using finite elements and generalized scattering matrix, IEEE Trans Antennas Propag 54 (2006), 899-907.